EFDA–JET–PR(09)19

T.W. Versloot, P.C. de Vries, C. Giroud, M.-D. Hua, M.N.A. Beurskens,
M. Brix, T. Eich, E. de la Luna, T. Tala, V. Naulin, K.D. Zastrow
and JET EFDA contributors

Effect of ELMs on Rotation and Momentum Confinement in H-mode Discharges in JET

Effect of ELMs on Rotation and Momentum Confinement in H-mode Discharges in JET

T.W. Versloot[1], P.C. de Vries[2], C. Giroud[2], M.-D. Hua[3], M.N.A. Beurskens[2], M. Brix[2], T. Eich[4], E. de la Luna[5], T. Tala[6], V. Naulin[7], K.D. Zastrow[2] and JET EFDA contributors*

JET-EFDA, Culham Science Centre, OX14 3DB, Abingdon, UK

[1]FOM Institute Rijnhuizen, Association EURATOM-FOM, Nieuwegein, the Netherlands
[2]EURATOM-UKAEA Fusion Association, Culham Science Centre, OX14 3DB, Abingdon, OXON, UK
[3]Imperial College, SW7 2BY, London, UK
[4]Max-Planck-Institut für Plasmaphysik, EURATOM Association, Garching D-85748, Germany
[5]Laboratorio Nacional de Fusión, Asociación EURATOM-CIEMAT, Madrid, Spain
[6]Association EURATOM-Tekes VTT, P.O. Box 1000, 02044 VTT, Finland
[7]Association EURATOM-Risø DTU, Fredericksborgvej 388, Roskilde, Denmarka
** See annex of F. Romanelli et al, "Overview of JET Results",*
(Proc. 22[nd] IAEA Fusion Energy Conference, Geneva, Switzerland (2008)).

Preprint of Paper to be submitted for publication in
Plasma Physics and Controlled Fusion

ABSTRACT.
The loss of plasma toroidal angular momentum and thermal energy by Edge Localised Modes (ELMs) has been studied in JET. The analysis shows a consistently larger drop in momentum in comparison to the energy loss associated to the ELMs. This difference originates from the large reduction in angular frequency at the plasma edge, observed to penetrate into to the plasma up to r/a~0.65 during large type-I ELMs. As a result, the time averaged angular frequency is lowered near the top of the pedestal with increasing ELM frequency, resulting in a significant drop in thermal Mach number at the edge. An increase in profile peaking of ion temperature and angular frequency is observed. At the same time the plasma confinement is reduced while the ratio of confinement times ($R_\tau = \tau_E/\tau_\varphi$) increases noticeably with ELM frequency. This change could be explained by the relatively larger ELM induced losses for momentum in combination with the observed longer build up time for the momentum density at the plasma edge.

1. INTRODUCTION

Momentum transport is an active area of research in many tokamaks due to the role of rotation and rotational shear in improving plasma confinement by e.g. turbulence suppression and Internal Transport Barriers (ITB). The physical processes driving the plasma momentum and energy transport are usually assumed to be closely related as in anomalous transport both result from similar underlying fluctuations [1]. Recent results from a large global database at JET [2] indeed showed a rough proportionality between energy and momentum confinement, as well as similar observations in other devices including ASDEX [3] and DIII-D [4]. However, the presence of a larger scatter does suggest a difference in the local behaviour between energy and momentum confinement and/or transport. At present it is however not well understood which parameters play a role in determining the plasma rotation profile while, at least at JET, it must also be noted that power and torque deposition are partially coupled in dominantly Neutral Beam Injection (NBI) heated plasmas [5]. As a result, the rotation profiles in current and future fusion devices remain difficult to predict accurately.

In general, the magnitude of the H-mode pedestal in combination with the large pedestal enclosed volume contributes significantly to the global momentum and energy content. In this way, the magnitude of the parameters and the plasma edge can play an important role in the overall observed confinement. Furthermore, recent findings [6, 7, 8] and supporting theory [9, 10] on the existence of a non-diffusive term in the momentum balance equation, the momentum pinch velocity Vp, show the importance of the edge rotation in contributing indirectly to the core confinement. It remains however largely unknown which processes determine the magnitude of the plasma rotation at the top of the pedestal.

One major influence on the pedestal is observed during Edge Localised Modes (ELMs), where the repetitive collapse of the H-mode pedestal causes an ejection of particles and energy through the last closed flux surface [11, 12]. Several models have been suggested to describe the ELM behaviour and to predict in particular the particle and energy losses in view of ITER [11, 13, 14]. Besides losses in particles and thermal energy, angular momentum can also be lost due to an ELM, although these losses may not necessarily be of a similar magnitude.

The ELM associated energy losses are found to vary in the range of 5-20% of the pedestal stored energy ($W_{ped} = 3/2 p_{ped} V_{ped}$ where pped and V_{ped} are the pedestal pressure and enclosed volume respectively) depending on plasma conditions [14, 15, 16]. It has been observed that the magnitude and nature of the energy losses, conductive and convective, changes with collisionality. At low collisionality the energy losses are found to be largest in size and mainly dominated by conductive losses, while at high collisionality the energy loss is smaller with the particle losses playing a more significant role. Additionally, the energy loss due to ELMs roughly scales inversely with ELM frequency (f_{ELM}) and the total loss appears to be constant at given plasma scenario and input power, irrespectively of collisionality [17].

The magnitude of the momentum losses however remains as of yet mostly unknown and the measurement of these losses is the main topic of this paper. Recent high temporal resolution measurements at the plasma edge in ASDEX indeed show a drop in angular frequency during a single ELM [18] with a reversed shear profile at the plasma boundary. Also, results from the JET rotation database [2] indicate a reduction in edge angular frequency with increasing ELM frequency while ion temperatures are less affected or even seen to increase due to the increase in applied input power. Both results would indicate a loss of momentum due to the ELM and in order to describe the global rotation profile it is therefore important to understand both the sources and sinks, in particular at the plasma edge.

This paper will investigate the momentum and thermal energy losses in JET H-mode plasmas with varying type-I ELM frequencies. The global plasma properties and confinement properties during several typical JET H-mode plasmas with increasing type-I ELM frequencies are presented first in section 2. These discharges have an increasing power input by NBI in order to alter the global energy and momentum content. The observed changes in the measured profiles of angular frequency ($\omega = v_\varphi/R$), temperature (Ti, Te) and density (ne) are discussed in section 3. In section 4, an estimate of the ELM induced momentum losses is presented using the observed radial drop profiles in all parameters and related to the measured energy losses. The relation of loss sizes with ELM frequency is discussed in section 5. In the last section, the main conclusions are summarised and discussed in which also the diagnostic measurement capabilities are taken into consideration in order to quantify the observed changes in confinement.

2. GLOBAL CONFINEMENT

It is found empirically that the energy confinement decreases with respect to the absorbed input power ($\tau_{IPB98(y,2)} \sim P^{-0.69}$ [19]) in plasmas with H-mode confinement. In order to study the coupling of energy and momentum confinement in different ELM regimes, a series of experiments was performed using a stepped neutral beam input power (PNBI) as is shown in figure 1. The discharge shown is a low triangularity ($\delta \sim 0.28$) type-I ELMy H-mode with a plasma current $I_p = 1.6$MA and toroidal field of $B_T = 1.6$T to obtain a low type-I ELM threshold in order to allow a large variation in f_{ELM} within the JET heating capacity. The input power was stepped up in three phases at Plow (4.5MW), P_{med} (7.5MW) and P_{high} (12MW). For this discharge, a steady-state phase in global energy content is reached roughly ~0.5s after both steps to Pmed and Phigh whereas at Plow the density profile continues to evolve after

the initial beam switch on. The particle recycling is also observed to increase at each step as can be seen in the increase in baseline of the D_α-radiation, however the edge density decreases slightly throughout the discharge and the net effect is thus assumed to be minimal. Each phase is characterised by type-I ELMs with increasing fELM of approximately 15, 30 and >60Hz respectively with an energy confinement enhancement factor (H98-y,2) ~ 1 [19] throughout the discharge.

The plasma rotation (v_φ) and ion temperature (T_i) profile have been measured with the core Charge Exchange Recombination Spectroscopy (CXRS) diagnostic with a measurement integration time of $\Delta t = 10$ms and spatial resolution in the order of 3-6cm increasing with radial position [20]. The ion species measured is that of the main impurity, C^{5+}, and it is assumed that all the ion species are in equilibrium. The outer most measurement point is located close to the pedestal top as can be interpreted from the electron density (n_e) profile measurements. The electron density (n_e) and temperature (T_e) are obtained from the High Resolution Thomson Scattering (HRTS) diagnostic which has a spatial resolution of 2cm with a 50Hz repetition frequency at a high temporal resolution of 10ns [21]. An alternative method for determining the electron density is by de-convolution of the line integration measurements, taking into account the magnetic equilibrium, which shows a good agreement with HRTS density measurements [22].

Combining these parameters, the global angular momentum (L_φ) and thermal energy (W_{th}) are defined by the volume integral over the full plasma radius as,

$$L_\varphi = \int n_e\, m_i m_{pe}\, R\, v_\varphi\, dV \tag{1}$$

$$W_{th} = \int 3/2\, k\, (n_i\, T_i + n_e\, T_e)\, dV \tag{2}$$

with mpe the atomic mass per electron and k as the Boltzmann constant. In the first two phases of the discharge both L_φ and Wth increase with P_{NBI} due to the coupling between torque and power deposition in NBI heating. However during the Phigh phase Wth continues to increase whereas L_φ reduces. This loss in momentum can be explained by a decrease in density, but also due to a large drop in angular frequency in the outer part of the plasma which happens even though significant additional torque is applied. This drop is better visualised in the radial profiles shown in figure 2 for each phase. The loss in density in the last phase is fully compensated by the power increase such that Wth increases due to the increase in temperature. Equivalent to the temperature increase, ω_φ in the core of the plasma increases due to the larger torque flux, leading to a steeper gradient of the rotation profile with respect to the pressure profile. Subsequently, a lowering in Mach number ($M_{th} = v_\varphi/\sqrt{(eT_i/m)}$) at the edge is seen from 0.3 to 0.15 (see also figure 1) while the core value remains roughly constant throughout the discharge.

Similar to the energy confinement, a decrease in the global momentum confinement ($\tau_\varphi = L_\varphi / (-dL_\varphi/dt)$) is seen in figure 1. In fact, the reduction in L_φ plays an important role in the change in confinement time ratio from $R_\tau = 0.8(\pm 0.2)$ at P_{low} to $R_\tau = 1.1(\pm 0.1)$ at P_{high}. A change in R_τ would indicate a difference in the behaviour of momentum losses in comparison to energy losses. Interesting to note is also the magnitude of L_φ and higher momentum confinement at P_{low}. Especially in this phase, the rotation and kinetic pressure at the plasma edge contribute significantly to L_φ and W_{th}

respectively due to the large elliptical volume. By separating the stored energy and momentum in a core and pedestal fraction, the edge R_τ is even seen to increase further to a maximum of $R_{\tau,ped}$ = 1.80±0.37 at P_{high}. This suggests that fluctuations at the pedestal play the dominant role in the observed behaviour. This would also be in agreement with the general observation in several plasma scenarios [2] that the pedestal conditions are an important factor in the observed global confinement. More evidently, it suggests that τ_φ does not scale as τ_E and that the losses for both channels therefore scale differently.

3. ELM DYNAMICS

In this section, we will focus on the losses associated with the ejection of energetic particles due to ELMs and their impact on the profiles of ω, $T_{i,e}$ and n_e. Besides direct losses, there are also several other possibilities that could additionally influence the radial profile. For example, a change in stiffness or threshold levels [23] or changes in pedestal characteristics [15] may play a role in these experiments by changing the nature of the pedestal or local transport, but these are left outside the scope of this analysis.

The dynamics of the ELM cycle are characterised by a fast drop (Δt = 0.1-0.2ms) in pedestal pressure gradient followed by a build up (in the order of 10-100ms) due to core transport until the critical gradient is reached and a successive ELM is triggered (see e.g. [16], [24]). Unfortunately, the measurement frequency of the CXRS at JET is not high enough to obtain detailed time resolved information during a single ELM crash period. Instead, we attempt to make a separation between pre and post phases relative to the ELM onset. For low frequency ELM cycles (typically less than 30Hz), a separation between pre- ELM ($-10ms < t\text{-}t_{ELM} < -5ms$) and post-ELM ($5ms < t\text{-}t_{ELM} <$ 10ms) rotation and ion temperature profiles can be made. At higher frequencies, the resolution of the CXRS measurement is limiting the separation due to the overlap of the pre- and post-ELM phases within the time integration period, effectively resulting in an ELM averaged measurement for fELM above 50Hz. A consequence is therefore that this method is unable to determine the absolute magnitude of the losses, but instead it can be used for a comparison of momentum and energy losses when taken at equal sampling rates and at equal time and spatial positions.

Using a coherent data sampling method as also used in [15], the average ω and T_i profiles around the ELM crash have been obtained for several fixed input power H-mode discharges (B_t = 2.2T, I_p = 2.MA) with type-I ELMs at an average f_{ELM}~20Hz (see figure 3). A clear drop in ω is observed from r/a~0.65 outwards while the T_i drop appears to be smaller and penetrating less deep. In a similar way, the change in ne and Te profile, measured by respectively HRTS and Electron Cyclotron Emission (ECE), can be interpreted on the same time and spatial grid. The HRTS profiles benefit from a high temporal resolution of 10ns but the resolution is limited by a 50Hz repetition rate. Therefore, the pre- and post-ELM density profile are obtained by averaging all density measurements within the set time windows. The maximum time resolution of the ECE is Δt~2ms and allows for a measurement much closer to the ELM crash. However, in order to compare the electron and ion profiles, the ECE signals are convoluted with a 10ms time integration window. This then results in a systematic underestimation of the change in profile due to the build up of the

profile within the first few milliseconds. This difference was found to be up as large as 15% of the pedestal size in several cases depending on plasma conditions and ELM size.

The radial position of the last measurement point from the core CXRS ($\rho_{cx} \sim <0.88\pm0.03$) is located close to the pedestal top ($\rho_{ped} = 0.92\pm0.02$) as derived from the density profile. The time evolution of several parameters obtained by ELM sorting is shown in figure 4. A 5ms time window around the ELM-crash is excluded from the analysis due to overlap between pre- and post-ELM periods. Natural variations in ELM dynamics result in a scatter of measurements and reflect the statistical uncertainty in estimating the average ELM induced drop. Nevertheless, a clear build up of the $T_{i,e}$ and ω can be seen. Notice in this case also the good agreement between T_e and T_i at the edge of the plasma, both in magnitude and time evolution, indicating a high collisionality between both species. However, it seems that the build up of the pedestal rotation does not always fully recover in between ELMs while this does seem to be the case for the density and temperature. Fitting an exponential growth function to the averaged time traces indicates a longer build up time for rotation ($\tau_\omega \sim 44$ms) compared to the ion temperature ($\tau_{Ti} \sim 21$ms) to return to 90% of the pre-ELM magnitude. To assess the relative changes, the radial drop profiles are shown in figure 5 normalised to the pre-ELM magnitude, defined as $\Delta A(\rho_i)/Apre(\rho_i)$ with ρ_i the location of each radial measurement of parameter $A = [\omega, T_i, T_e, n_e]$. The data of several identical discharges has been averaged and the errorbars represent the spread in the distribution of drop sizes obtained in averaging all ELMs. A consistently larger drop in angular frequency is observed relative to the ion temperature at the pedestal, $\Delta\omega/\omega_{pre} = 45\pm7\%$, $\Delta T_e/T_{e,pre} = 20\pm6\%$ (from HRTS and ECE), $\Delta T_e/T_{e,pre} = 20\pm4\%$ (from CXRS) and density, $\Delta n_e/n_{e,pre} = 12\pm4\%$ (from HRTS). The density profile obtained by de-convoluting the line integrated density shows a good agreement with the HRTS data, which increases certainty on the measured density drop.

Taking into account the measurement uncertainty, the low limit on the measurable drop size is empirically set at 5% for all diagnostics. The radial extent of the ELM losses is therefore defined by the radial position at which the relative change is below this limit. The ELM affected area in the rotation profile then extends up to $\rho \sim 0.65$ into the plasma, while both the electron and ion temperature and electron density penetrate less deep, $\rho \sim 0.80$. It is generally observed in JET baseline ELMy H-mode plasmas that the ELM penetration depth for density and temperature does not extent beyond $\rho \sim 0.80$ as was reported in [11, 15]. Only in advanced tokamak scenarios, the penetration was seen to extent further into the plasma [15, 25].

It must be noted that the time period between the ELM crash and the first post-ELM measurement is off the same order as diffusive transport time scales, O(ms). Within this time, a significant part of the post-ELM profile can be regenerated by transport from the plasma core thereby decreasing the observed ELM affected area. Recent work at ASDEX [18] from high resolution CXRS measurements at the plasma edge does show profile evolution time scales in the order of milliseconds which could affect momentum and energy differently.

4. MOMENTUM AND ENERGY LOSSES

The angular momentum and thermal energy are conserved quantities and a different behaviour in these losses would also suggest a difference in the underlying transport. The momentum and energy

drop are calculated by determining the pre- and post-ELM profile using equations 1 and 2. Figure 6a shows the results for a selection of discharges in which all the necessary diagnostics were available. It was found that for all discharges the momentum drop is consistently larger than the drop in thermal energy. The losses are shown normalised to the pre-ELM value and thus reflect the global loss fraction. In all cases, this fraction is largest for momentum losses compared to the energy losses by roughly a factor 1.5. This difference is completely due to the contribution and radial extent of the drop in angular frequency as particle losses contribute equally to both parameters. The ion density was estimated from the electron density by a single carbon impurity correction on the time averaged Z_{eff} as determined from bremsstrahlung measurements. Unfortunately, this indirect method has a relatively large uncertainty, however any possible increase in Z_{eff} during the ELM crash will further decrease the main ion density and hence only increase the difference.

For the similar discharges presented in the previous section (red dots), the average loss fraction is $\Delta L_\varphi/L_\varphi = 9\pm1\%$ in comparison to $\Delta W_{th}/W_{th} = 5\pm1\%$. The errors in this case have been derived from the statistical averaging in the data sorting method. The largest contribution of these losses originates from the mid to edge region and therefore the losses are usually normalised to the pedestal stored value with $W_{th,ped} \sim 0.3\text{-}0.4W_{th}$. In this case, the loss fractions increase to $\Delta L_\varphi/L_{\varphi,ped} = 22\pm3\%$ and $\Delta W_{th}/W_{th,ped} = 16\pm5\%$ respectively. The magnitude for the energy loss in these low collisionality discharges is in good quantitative agreement with earlier analysis [11, 14, 15, 24] and also with infrared-camera measurements [26]. Furthermore, the fraction of thermal energy for electrons was found to be roughly equal to the ion thermal energy when including Z_{eff}. This indicates that both species have reached kinetic equilibrium such that the energy losses are not concentrated in either electrons or ions. A difference could contribute to a discrepancy with the momentum losses which is completely carried by the ions.

The analysis presented here focuses only thermal losses. To assess the contribution of fast particles, the drop is diamagnetic energy is shown versus the thermal energy drop for all discharges in figure 6b. A good agreement is found which implies that the energy losses are mainly caused by the thermal particles if one assumes poloidal symmetry throughout the ELM crash. The combination of large momentum losses with a long build up time effectively reduces the time averaged momentum. Naturally, this depends on ELM frequency and is smallest in the case of low-frequency ELMs where the time in between ELMs is long compared to the build up time. In these cases, the momentum confinement time is also observed to be higher than the energy confinement time (see figure 1). This suggests an improved inter-ELM confinement for momentum and a relation between ELM frequency, or inter-ELM time, and confinement time ratio.

5. ELM FREQUENCY DEPENDENCE

With the increase in ELM frequency, the inter-ELM period is reduced and the ELM size generally becomes smaller [11]. Furthermore, with the decrease in ELM size, the losses of momentum and energy are reduced although it is observed in several studies that the total energy loss remains a constant fraction of the input power ($\Delta W_{tot} = f_{ELM}\,\Delta W_{ELM} = c_1 P$) [17]. In the study presented here, the largest observed drop in momentum was seen in discharges with a low ELM frequency (6Hz)

but relatively large ELM sizes (250kJ). In order to study the effect of ELM frequency on the size of the momentum losses, a series of discharges was selected with similar configuration but with the application of ELM frequency mitigation by vertical kicks [27]. The nature of this method is outside of the scope of this analysis and assumed only to affect the ELM frequency and size. Figure 7a shows the normalised momentum loss ($\Delta L_\varphi/L_\varphi$) versus the average ELM frequency observed in the time windows of all the discharges presented in this study. The decay of the drop size with f_{ELM} suggests that, similar to the behaviour for the energy losses, the total momentum loss might also be a constant fraction of the total external sources. However, the range in ELM frequencies is unfortunately limited by the diagnostic time resolution. The set of discharges shown here consists of a wide range of applied power and torque at different plasma configurations but show a consistent behaviour in the observed losses. However, to account for the variations in confinement time, figure 7b shows the loss fraction versus normalised frequency ($f_{ELM}\tau_{\varphi,E}$) for both energy and momentum. The loss fraction can be approximated by a constant in the order of c_1~0.3 for energy and c_2~0.4 for momentum, although with a relatively large uncertainty due to the scatter.

DISCUSSION AND CONCLUSIONS

In this paper, the effect of ELMs on the losses of momentum and thermal energy has been studied. The change in ELM averaged confinement has been discussed with the assumption that the external power and torque deposition are well known and remain constant throughout the ELM phases. The effect of particle transport is assumed to be minimal, although it does cause a limitation on the derived drop size when also considering the diagnostic time resolution. Nevertheless, a comparison on similar time scales and resolutions does provide an insight in the underlying processes by placing a lower limit on the ELM associated losses. Furthermore, it must be noted that the magnetic equilibrium is assumed to be quickly reestablished after the ELM-crash. This might not necessary be the case as both fast fluctuations in plasma shape and the sharp increase in D_α radiation are indications of a change in equilibrium and the possible enhancement of external drag forces by e.g. charge exchange friction with cold neutrals at the edge. These effects among others could also influence the momentum pedestal. However, here we have not investigated the size of the pedestal, but instead have focused directly on the magnitude of the observed losses by ELMs.

In general, a consistent change in confinement time ratio is observed with ELM frequency where the momentum confinement time is higher in the region of low frequency ELMs ($R_\tau > 1$) and lower ($R_\tau < 1$) at high f_{ELM}. A comparison of the ELM related losses revealed a larger loss in angular momentum in comparison to thermal energy in several H mode discharges at varying operating conditions. The magnitude of the energy losses was found to be in good agreement with previous results. The average losses obtained during moderate ELM frequency (f_{ELM} ~ 20Hz) and low collisionality was found to be approximately $\Delta L_\varphi/L_{\varphi,ped} = 22\pm3\%$ of the pedestal stored fraction in comparison to $\Delta W_{th}/W_{th,ped} = 16\pm5\%$. With increasing fELM the magnitude of the losses is reduced as the ELM size decreases, however the total loss of momentum appears to be a constant fraction of the total applied external source, similar to observations for the scaling of energy losses. The ELMs induce a periodic loss of energy and momentum which effectively reduces the time averaged

confinement. A significant change in confinement is observed when the build up time is long compared to the inter-ELM time length. It was observed that the build up time of the rotation pedestal is slightly longer compared to the temperature. In fact, for relatively slow ELMs ($1/f_{ELM} >> f_{rise}$) the initial losses can be completely regenerated before the subsequent ELM while with increasing fELM the rotation is first unable to fully recover to similar pre-ELM levels even though additional external torque is being applied. As a result, the momentum density at the edge is effectively lowered due to the decrease in time averaged rotation. This mechanism thus offers a possible explanation for the observed changes in the global confinement time ratio as the energy confinement appears less affected due to the smaller losses.

Although global momentum and energy confinement are clearly related, the local behaviour seems to influence momentum and energy differently. This seems especially the case near the pedestal and edge region where additional sources or sinks might play a more profound role. In relation to the present momentum pinch studies, this process would then also contribute to the magnitude of the inwards momentum flux by the change in the pedestal rotation velocity. In this way, the pedestal contributes both directly to the global confinement by the large enclosed plasma volume as well as indirectly through the inwards momentum flux to the plasma core. For example, in the discharge presented in section 1 of this paper, L_φ remained roughly constant although the input torque was significantly increased over the entire radial profile during the stepped NBI while only the edge rotation was noticeably reduced. In order to understand and accurately predict the global confinement properties it is therefore necessary to further investigate all the processes affecting the plasma boundary to assess their influence on both local and global plasma behaviour.

ACKNOWLEDGEMENTS

This work, supported by the European Communities under the contract of Association between EURATOM, FOM and UKAEA, was carried out in the framework of the European Fusion Programme. The views and options expressed herein do not necessarily reflect those of the European Commission.

REFERENCES

[1]. N. Mattor, P.H. Diamond, Physics of Fluids **31** (1988) 1180
[2]. P.C. de Vries, et al., Nuclear Fusion **48** (2008) 065006.
[3]. D. Nishjima, et al., Plasma Physics Controlled Fusion **47** (2005) 89
[4]. W.M. Solomon, et al., Plasma Physics Controlled Fusion **48** (2007) B313
[5]. K.-D. Zastrow, et al., Nuclear Fusion **38** (1998) 257.
[6]. M. Yoshida, et al., Nuclear Fusion **47**, 856 (2007)
[7]. W.M. Solomon, et al., Nuclear Fusion **49** (2009) 085005
[8]. T. Tala, et al., Physics Review Letters **102** (2009) 045010
[9]. A.G. Peeters, C Angioni, D. Strintzi, Physics Review Letters **98** (2007) 265003
[10]. T.S. Hahm, et al., Physics of Plasmas **14** (2007) 072302
[11]. A. Loarte, et al., Plasma Physics Controlled Fusion **44** (2002) 1815

[12]. A. Kirk, et al., Journal of Physics: Conference Series **123** (2008) 012011
[13]. E. Solano, et al., Nuclear Fusion 48 (2008) 065005
[14]. K. Kamiya, et al., Plasma Physics Controlled Fusion **48** (2006) A131
[15]. M.N.A. Beurskens, et al., *accepted for publication in Nucl. Fusion*
[16]. A. Loarte, et al., Plasma Physics Controlled Fusion **45** (2003) 1549
[17]. H. Urano, et al., Plasma Physics Controlled Fusion **45** (2003) 1571
[18]. T. Putterich, et al., Physics Review Letters **102** (2009) 025001
[19]. D.C. McDonald, et al., Nuclear Fusion **47** (2007) 147
[20]. C. Giroud, et al., Review Scientific Instruments **79** (2008) 10F525
[21]. R. Pasqualotto, et al., Review Scientific Instruments **75** (2004) 3891
[22]. M. Brix, et al., *to be submitted*
[23]. P. Mantica, et al., Physics Review Letters **102** (2009) 175002
[24]. N. Oyama, et al., Plasma Physics Controlled Fusion **44** (2004) 582
[25]. M.N.A. Beurskens, et al., Nuclear Fusion **48** (2008) 095004
[26]. T. Eich, et al., Plasma Physics Controlled Fusion **49** (2007) 573
[27]. E. de La Luna, et al., Proc. 35th European Physical Society Conf. on Plasma Physics and Controlled Fusion (Sofia, Bulgaria, 29 June –3 July 2009) P5.174

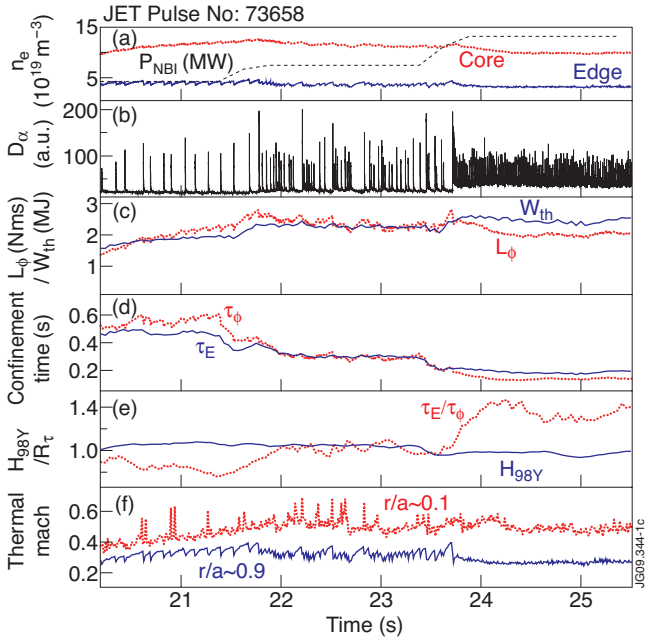

Figure 1: Evolution of plasma properties during a stepped power discharge with a) Neutral Beam power (black) and core/edge (red/blue) line integrated density. b) $D\alpha$-radiation showing an increase in f_{ELM}. c) Global angular momentum, $L\varphi$, and thermal energy, W_{th}. d) Confinement time e) Ratio of confinement times (red) and H98Y-factor (blue). f) Thermal Mach number near the plasma core (red) and pedestal (blue) determined from ion temperature.

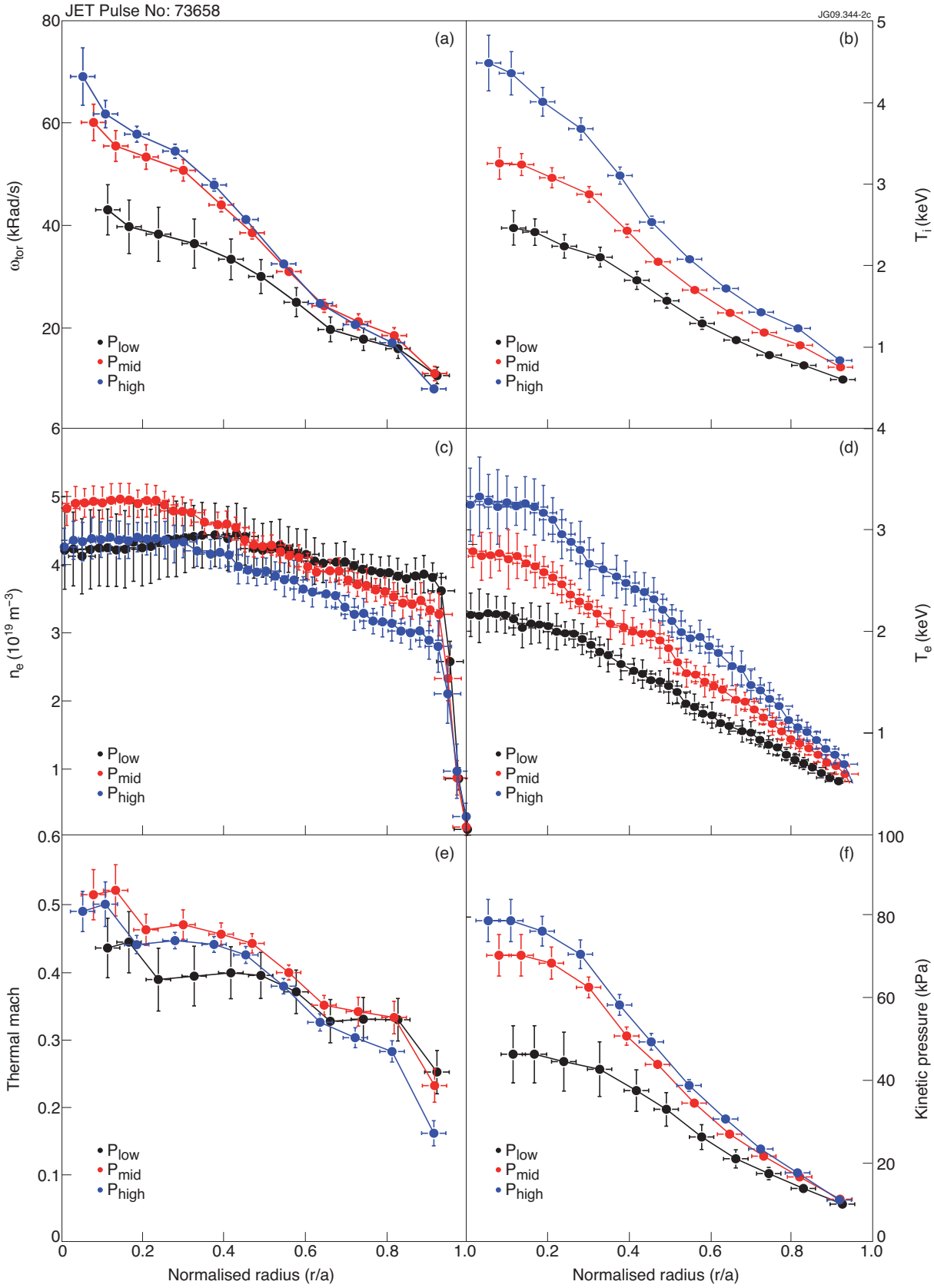

Figure 2: Averaged plasma profiles for a) angular frequency b) ion temperature c) electron density and d) electron temperature e) Mach numbers and f) kinetic pressure at stepped NBI phase.

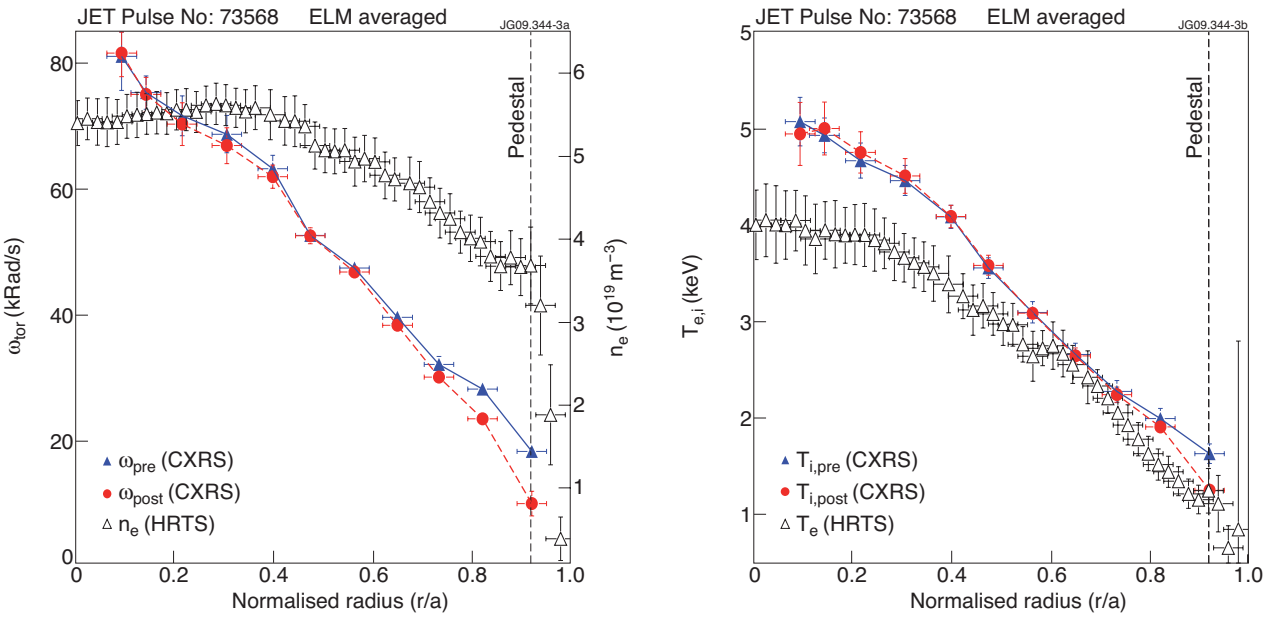

Figure 3: ELM averaged (nELM=82) radial profiles and statistical uncertainty of pre- and post- ELM profile for angular frequency (left) and ion temperature (right). The pedestal location is shown as derived from the average HRTS density profile. The errorbars denote the observed fluctuations of the profile within the selected time window.

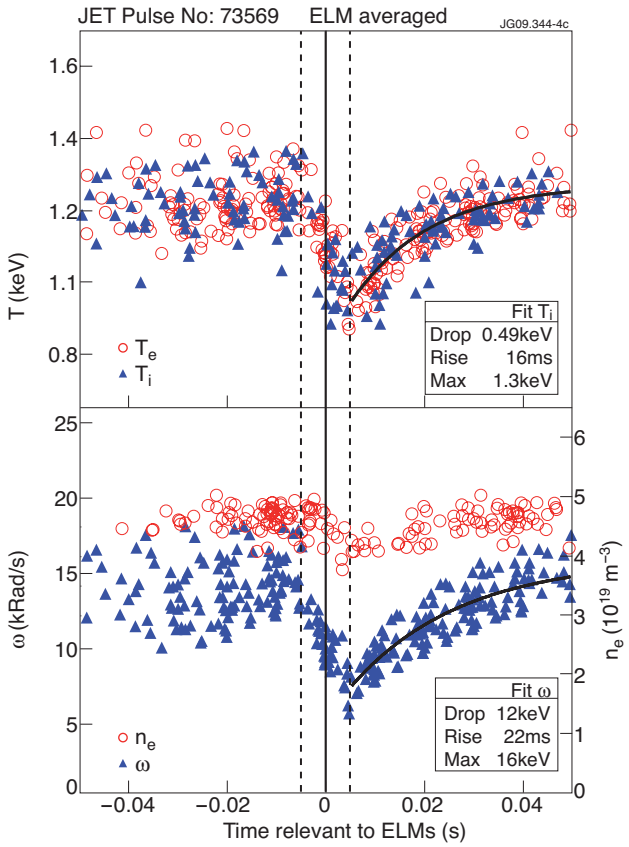

Figure 4: ELM averaged time trace obtained with coherent data sorting for ion (blue) and electron (red) temperature near the pedestal location (top figure). In the bottom figure, angular frequency (blue) and electron density (red). An exponential growth function is fitted to the post-ELM time profile indicating a faster build up of the temperature (τ_{T_i}~21ms) in comparison to the rotation (τ_{ω} ~ 44ms) to return to 90% of the pre-ELM size.

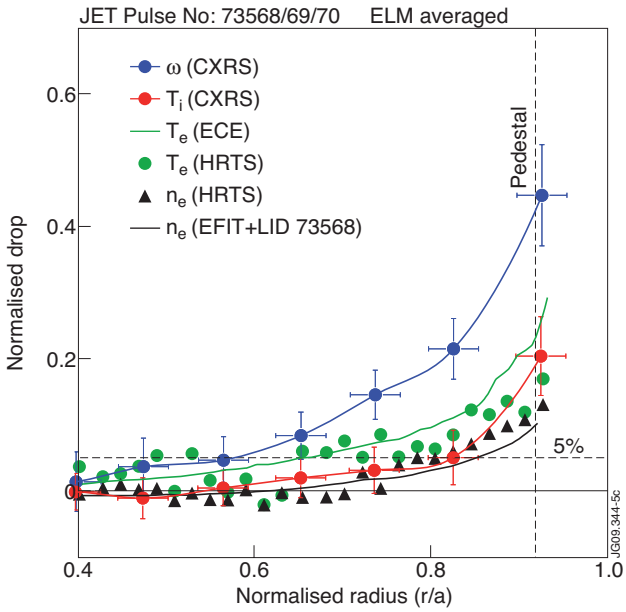

Figure 5: Radial profile of the parameter drop normalised to the pre-ELM magnitude for angular frequency (blue), ion temperature (red), electron temperature (green) and electron density (black). The temporal resolution and measurement time relative to the ELM onset is set equal for each signal. Notice the large drop in angular frequency together with a deeper radial penetration.

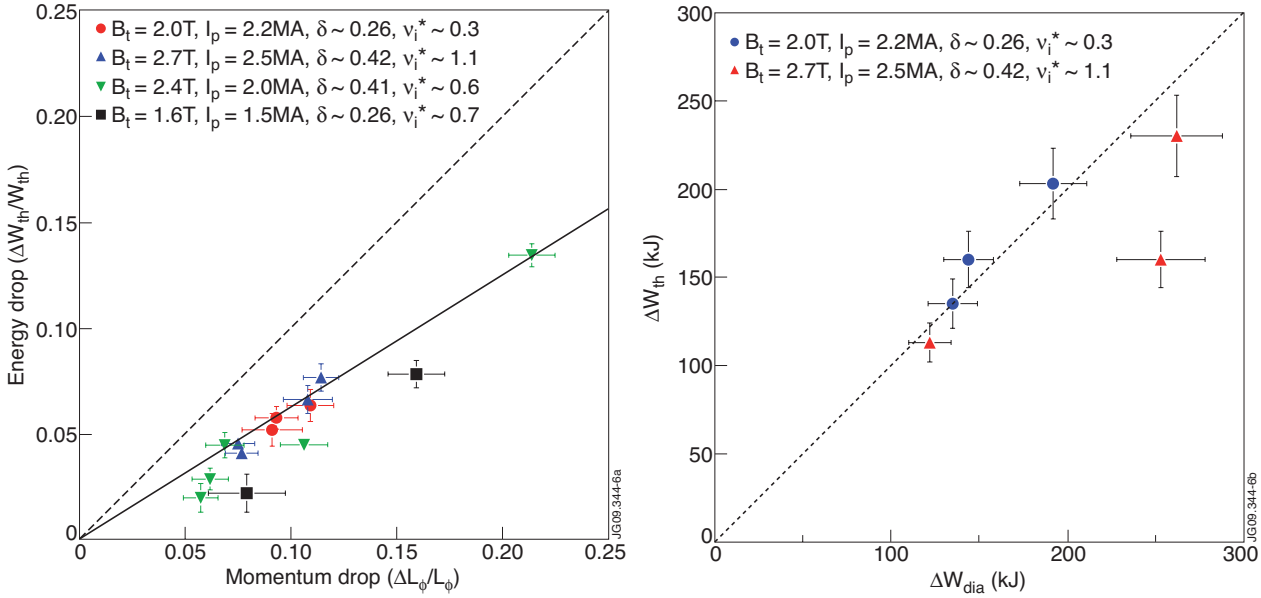

Figure 6: (left) Normalised thermal energy drop versus the normalised momentum drop in several different plasmas discharges at varying operating conditions. The drop in angular momentum is consistently larger compared to the thermal energy by roughly a factor 1.6 (full line) (right) Thermal energy drop versus diamagnetic energy loss. The errors are estimated from ELM averaging.

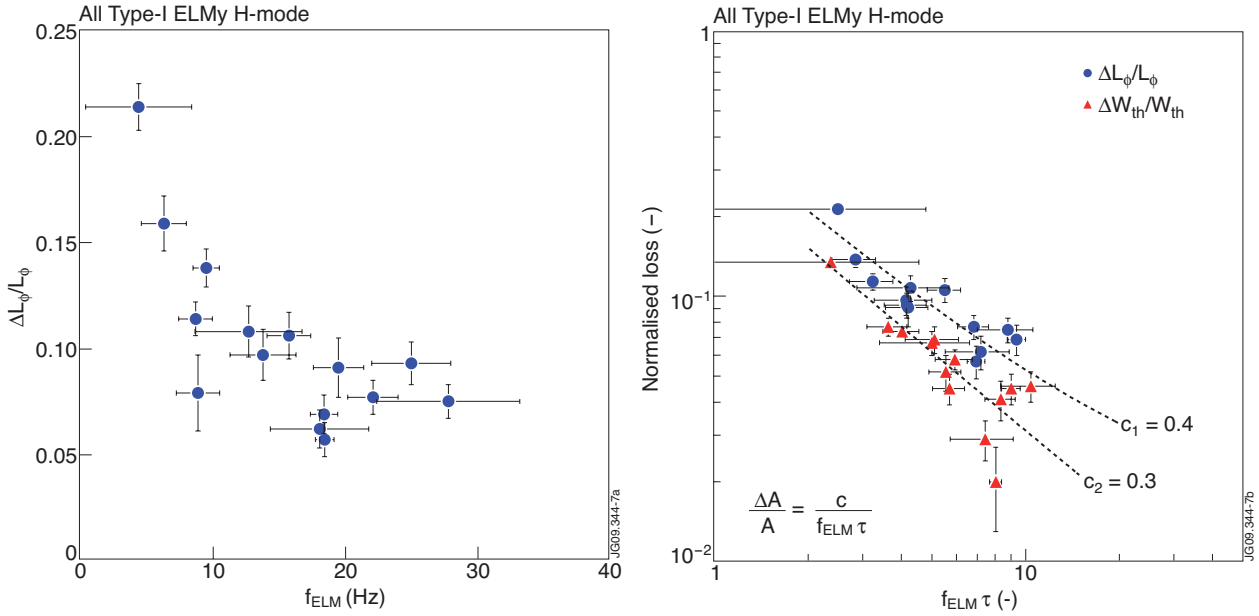

Figure 7: (left) Scaling of normalised angular momentum loss as a function of ELM frequency for all discharges. The loss per individual ELM reduces with f_{ELM}. (right) Normalised momentum (blue) and energy (red) loss versus normalised fELM. Both the total momentum and energy loss can be expressed as a constant fraction of the global plasma content, with the momentum loss consistently larger than the thermal energy loss.